Weierstraß-Institut
für Angewandte Analysis und Stochastik
Leibniz-Institut im Forschungsverbund Berlin e. V.

Preprint ISSN 2198-5855

Quantum dynamics of coupled excitons and phonons in chain-like systems: Tensor train approaches and higher-order propagators

Patrick Gelß[1, 2], Sebastian Matera[1,3], Rupert Klein[1], Burkhard Schmidt[1,4]

submitted: February 17, 2023

[1] Institut für Mathematik
Freie Universität Berlin
Arnimallee 3–9
14195 Berlin, Germany
E-Mail: gelssp@zedat.fu-berlin.de
matera@math.fu-berlin.de
rupert.klein@math.fu-berlin.de
burkhard.schmidt@fu-berlin.de

[2] Zuse-Institut Berlin
Takustr. 7
14195 Berlin, Germany
E-Mail: gelss@zib.de

[3] Fritz-Haber-Institut der Max-Planck-Gesellschaft
Faradayweg 4–6
14195 Berlin, Germany
E-Mail: matera@fhi.mpg.de

[4] Weierstrass Institute
Mohrenstr. 39
10117 Berlin, Germany
E-Mail: burkhard.schmidt@wias-berlin.de

No. 2995
Berlin 2023

2020 *Mathematics Subject Classification.* 35L05, 65D40, 65M70, 65P10, 81Q05.

2010 *Physics and Astronomy Classification Scheme.* 02.30.Jr, 02.60.Cb, 03.65.Ge, 07.05.Tp, 63.20.D-, 63.20.kd, 71.35.Aa.

Key words and phrases. Numerical quantum mechanics, Schrödinger equations, tensor train decompositions, symplectic integrators, exciton-phonon-coupling, Fröhlich–Holstein Hamiltonian.

Funded by the Deutsche Forschungsgemeinschaft (DFG, German Research Foundation) under Germany's Excellence Strategy – The Berlin Mathematics Research Center MATH+ (EXC-2046/1, project ID: 390685689) and by the CRC 1114 "Scaling Cascades in Complex Systems" funded by the Deutsche Forschungsgemeinschaft (project ID: 235221301, project B06). Felix Henneke (FU Berlin) is acknowledged for insightful discussions and Jerome Riedel for valuable help with the implementation of the WaveTrain Python codes. Moreover, the authors would like to thank the HPC Service of ZEDAT, FU Berlin, for generous allocation of computing resources.

Edited by
Weierstraß-Institut für Angewandte Analysis und Stochastik (WIAS)
Leibniz-Institut im Forschungsverbund Berlin e. V.
Mohrenstraße 39
10117 Berlin
Germany

Fax: +49 30 20372-303
E-Mail: `preprint@wias-berlin.de`
World Wide Web: `http://www.wias-berlin.de/`

Quantum dynamics of coupled excitons and phonons in chain-like systems: Tensor train approaches and higher-order propagators

Patrick Gelß, Sebastian Matera, Rupert Klein, Burkhard Schmidt

Abstract

We investigate the use of tensor-train approaches to the solution of the time-dependent Schrödinger equation for chain-like quantum systems with on-site and nearest-neighbor interactions only. Using the efficient SLIM representation for low-rank tensor train representations of quantum-mechanical Hamiltonians, we aim at reducing the memory consumption as well as the computation costs, in order to mitigate the curse of dimensionality as much as possible. As an example, coupled excitons and phonons modeled in terms of Fröhlich–Holstein type Hamiltonians are studied here. By comparing our tensor-train based results with semi-analytical results, we demonstrate the key role of the ranks of tensor-train representations for quantum state vectors. Both the computational effort of the propagations and the accuracy that can be reached crucially depend on the maximum number of ranks chosen. Typically, an excellent quality of the solutions is found only when the ranks exceeds a certain value. That threshold, however, is very different for excitons, phonons, and coupled systems. One class of propagation schemes used in the present work builds on splitting the Hamiltonian into two groups of interleaved nearest-neighbor interactions which commutate within each of the groups. In addition to the first order Lie–Trotter and the second order Strang–Marchuk splitting schemes, we have also implemented the 4-th order Yoshida–Neri and the 8-th order Kahan–Li symplectic compositions. Especially the latter two are demonstrated to yield very accurate results, close to machine precision. However, due to the computational costs, currently their use is restricted to rather short chains. Another class of propagators involves explicit, time-symmetrized Euler integrators. Building on the traditional second order differencing method, we have also implemented higher order methods. Especially the 4-th order variant is recommended for quantum simulations of longer chains, even though the high precision of the splitting schemes cannot be reached. Moreover, the scaling of the computational effort with the dimensions of the local Hilbert spaces is much more favorable for the differencing than for the splitting schemes.

1 Introduction

Excitonic energy transport (EET), i.e., the transport of electronic energy without net charge is of paramount importance in many biological and technological systems. In particular, the efficiency of the conversion of light into chemical or electric energy crucially depends on it [54, 45]. For example, in photovoltaic devices the transport of energy from the region of primary excitation to the charge separating interfaces has to be fast enough to compete with radiative and non-radiative decay channels, most prominently the recombination of electrons and holes. The efficiency of EET is strongly affected by the coupling of electronic excitations to (intramolecular and/or intermolecular) vibrational degrees of freedom [68, 81]. The simplest theoretical approaches to this exciton-phonon coupling (EPC) are based on the assumption of chain-like, quasi-1D arrangements. Examples relevant for semiconducting

DOI 10.20347/WIAS.PREPRINT.2995

materials are lattice vibrations in 1D molecular crystal models or various stretching, bending, and/or torsional motions in conjugated polymer chains. The "dressingöf excitons by vibrations in these classes of systems is often described in terms of Holstein or Fröhlich type Hamiltonians. Originally developed for polarons [14], these model Hamiltonians, or extensions thereof, are routinely used in a variety of applications, ranging from vibrational energy transport in helical proteins [13, 70, 27] up to electronic energy transport in conjugated polymer chains [4, 17]. Despite of the apparent simplicity of the Fröhlich–Holstein type systems, their quantum dynamics still poses many open questions, as noted in the abstract of Ref. [14]: “It is remarkable how the Fröhlich polaron ... has resisted full analytical or numerical solution ... since $\sim$1950, when its Hamiltonian was first written. The field has been a testing ground for analytical, semi-analytical and numerical techniques, such as path integrals, strong-coupling perturbation expansion, advanced variational, exact diagonalization (ED) and quantum Monte Carlo (QMC) techniques.” Hence, the study of Fröhlich–Holstein type systems as models for exciton dynamics in the presence of EPC remains an intriguing and timely research field.

Essentially, the problems of theoretical studies of EPC are due to the quantum dynamical treatment required for the above-mentioned models, i.e., solutions of time-dependent Schrödinger equations (TDSE) in many dimensions. Quantum dynamical simulations to solve the TDSE with conventional methods eventually become unfeasible when increasing the number of dimensions [44]. One way to circumvent this so-called *curse of dimensionality* is to resort to mixed (or hybrid) quantum-classical methods. There, only the electronic degrees of freedom are treated quantum-mechanically, while the nuclear (ionic) degrees of freedom are treated classically, typically justified by the small electron to ion mass ratio [48]. The most basic of these hybrid methods is the quantum-classical Ehrenfest approach which plays an important role, e.g., in the Davydov soliton theory for EET in helical proteins [13, 70, 27]. Apart from the classical approximation, the main limitation of Ehrenfest dynamics is that it builds on a mean-field coupling of the two sub-systems [6, 56, 11]. This bottleneck is overcome in surface hopping trajectory approaches, where non-adiabatic transitions are approximately treated by stochastic hopping of trajectories between different (diabatic or adiabatic) energy states [76]. Even though surface hopping trajectory techniques have lately been used a lot in studying the photo-induced physics and chemistry of EET [79, 55, 21], the validity of the underlying approximations of quantum-classical dynamics is not always clear. In particular, for EET in organic semiconductors, there is sometimes no clear distinction between slow and fast degrees of freedom [81].

The focus of the present work is on methods for fully quantum-mechanical approaches to treat coupled excitons and phonons. In the literature, reports of such simulations are scarce. One example are quantum dynamical investigations of the related problem of formation of polarons in crystals where variational techniques for representing quantum state vectors were used [74, 46]. In more recent work, structure and dynamics of excitons in π-conjugated polymers were investigated, with emphasis on coupling to the torsional dynamics of the chain [4, 17]. In those studies, the multi-configurational time-dependent Hartree (MCTDH) method and its multi-layer (ML) extension were used, which are known as highly efficient algorithms for quantum dynamics in high dimensions [3, 53].

In recent years, the interest in low-rank tensor decompositions has been growing steadily. The potential of different tensor formats like the canonical format [32], the Tucker format [75], and particularly the tensor-train (TT, aka matrix product states, MPS) format [59] for mitigating the curse of dimensionality has been shown in various application areas. So far, tensor decomposition techniques have been used in the fields of, e.g., quantum mechanics [57, 7, 8, 26], neuro-imaging [37, 9, 18], system identification [43, 23, 38], and supervised learning [72, 42, 39], just to name a few. In previous work, we proposed TT-based techniques for numerically solving the time-independent Schrödinger equations (TISE) for coupled excitons and phonons [22]. There, it has been demonstrated that high-dimensional quantum systems comprising only NN interactions may be simulated and analyzed without an exponential scaling of the memory consumption and/or computational effort by using so-called SLIM decompositions [24]. Note that the underlying TT representations are a special case of the hierarchical Tucker format [28], which is equivalent to the wave function representation in the multi-layer (ML) variant of MCTDH. In recent comparisons of the efficiency of both methods for calculating ground states of chains of molecular rotors, it has been found, that TT/MPS techniques are less time- and memory-consuming than the state-of-the-art implementation of ML-MCTDH [52, 71].

In the present work, we want to exploit low-rank TT decompositions of quantum state vectors and Hamiltonian matrices for the case of the time-dependent Schrödinger equation (TDSE). In addition to previously published time integrators for TTs using projectors onto the tangent space of the tensor manifold [50, 51, 29], also symmetric Euler differencing schemes [10] and split operator techniques [19, 63] have been suggested recently for use with TT representations [57, 78, 61]. Being explicit and easy to implement, these two integrators have been in use since the early days of numerical quantum dynamics [47]. Our goal is to investigate them along with their higher-order variants, see Sec. 3. There, the various time integrators are subjected to rigorous tests for realistic models of excitons, phonons, and exciton-phonon-coupling. To that end, we are not only considering their ability to conserve norm and energy but also how accurately they can reproduce semi-analytic propagations which are available for special cases, see Sec. 4. On the one hand, our focus will be on the scaling of the numerical effort with the chain length and the Hilbert space dimensions, thus assessing the propagators for use in simulations of large systems. On the other hand, we will elucidate on the use of higher-order methods in comparison to lower-order ones in the context of low-rank TT representations of high-dimensional wave functions. In particular, we will address the question whether the increased costs for each propagation step will be compensated by the possibility to use larger step sizes, and, hence, a smaller number of steps, while obtaining solutions with the same accuracy. Note that implicit schemes such as the trapezoidal rule or the midpoint rule are not considered here. Even though they offer the advantage of conserving energy, their computational effort is unfavorable because they involve solutions of large-scale linear systems of equations. While this is in principle possible for TTs by virtue of the alternating linear scheme [33], which is also used in our previous TISE study [22], it is computationally too expensive to do this in every time step.

2 Model Hamiltonians

In the present work, we use Fröhlich–Holstein type Hamiltonians to describe the dynamics of excitons and phonons. With the coupling of the two subsystems assumed to be linear, these can be considered as the simplest models of EPC in organic semiconductors [68, 81]. Originally developed for electrons in a polarizable lattice [14], these models, partly with minor modifications, are also known as Huang-Rhys, or Peierls models. There is also a close analogy to Davydov models describing the interaction of the amide I vibrations and the hydrogen bond stretching in α-helices of proteins [70, 27].

Here, we restrict ourselves to the consideration of effectively one-dimensional, linear chains comprising N exciton-supporting sites assuming NN interactions only, see also our previous work [22]. Such models are suitable for the description of two classes of systems [54, 31] in the context of photovoltaics applications. First, in conjugated polymer chains without major kinks or turns, the excitonic sites interact with each other mainly via a Dexter mechanism "through bond") [15]. Second, in crystals of polycyclic aromatic molecules, the coupling of excitons occurs mainly in the direction perpendicular to the planes of the stacked molecules, governed by the Förster mechanism ("through space") [16].

The total Hamiltonians for the coupled excitons and phonons can be written as

$$H = H^{(\mathrm{ex})} \otimes \mathbb{I}^{(\mathrm{ph})} + \mathbb{I}^{(\mathrm{ex})} \otimes H^{(\mathrm{ph})} + H^{(\mathrm{epc})} \tag{1}$$

with the superscripts (ex), (ph), and (epc) standing for excitons, phonons and their coupling, respectively, while the $\mathbb{I}$ are the respective identity operators. Note that atomic units with $\hbar = 1$ are used throughout this work.

Restricting ourselves to a chain of two-state-systems, the excitonic Hamiltonian for a linear or cyclic system of N (identical or not) sites is given in terms of (bosonic) exciton raising, $b_i^\dagger$, and lowering, b_i, operators

$$H^{(\mathrm{ex})} = \sum_{i=1}^{N} \alpha_i b_i^\dagger b_i + \sum_{i=1}^{N} \beta_i \left(b_i^\dagger b_{i+1} + b_i b_{i+1}^\dagger \right) \tag{2}$$

with local (ön site") excitation energies α_i for site i. The nearest-neighbor (NN) coupling energies β_i between site i and $i+1$, also known as transfer or hopping integrals, determine the exciton delocalization and mobility. Here and throughout the following, the last summand ($i = N$) of the NN coupling term (with indices $i+1$ replaced by 1) is intended for systems with periodic boundary conditions only and is deleted otherwise.

The vibrational (phononic) Hamiltonian for a one-dimensional lattice can be written in terms of masses m_i, displacement coordinates R_i, and conjugated momenta P_i in harmonic approximation

$$H^{(\mathrm{ph})} = \frac{1}{2} \sum_{i=1}^{N} \frac{P_i^2}{m_i} + \frac{1}{2} \sum_{i=1}^{N} m_i \nu_i^2 R_i^2 + \frac{1}{2} \sum_{i=1}^{N} \mu_i \omega_i^2 \left(R_i - R_{i+1} \right)^2 \tag{3}$$

where each site i is restrained to oscillate around its equilibrium position by a harmonic potential with frequency ν_i and where the NN interactions between sites i and $i+1$ are modeled by harmonic oscillators with frequency ω_i and corresponding reduced masses $\mu_i = m_i m_{i+1} / (m_i + m_{i+1})$. Note that the frequencies ν_i and ω_i are assumed to be independent of the excitonic state of the system.

In parallel with the treatment of the excitons, we introduce second quantization also for the phononic Hamiltonian of Eq. (3) resulting in

$$H^{(\mathrm{ph})} = \sum_{i=1}^{N} \tilde{\nu}_i \left(c_i^\dagger c_i + \frac{1}{2} \right) - \sum_{i=1}^{N} \tilde{\omega}_i \left(c_i^\dagger + c_i \right) \left(c_{i+1}^\dagger + c_{i+1} \right) \tag{4}$$

where raising and lowering operators of (local) vibrations of site i are indicated by $c_i^\dagger$ and c_i, respectively, and where for the effective frequencies of single site and NN pair vibrations the following expressions

$$\tilde{\nu}_i = \sqrt{\nu_i^2 + \frac{m_{i-1}}{m_i + m_{i-1}} \omega_{i-1}^2 + \frac{m_{i+1}}{m_i + m_{i+1}} \omega_i^2} \tag{5}$$

$$\tilde{\omega}_i = \frac{\mu_i \omega_i^2}{2\sqrt{m_i \tilde{\nu}_i m_{i+1} \tilde{\nu}_{i+1}}} \tag{6}$$

have been found where for linear systems without periodic boundary conditions the second or third term under the square root of Eq. (5) is omitted for the first ($i = 1$) or last ($i = N$) site, respectively.

Linear models for the coupling of excitons and phonons can be formulated in terms of a Fröhlich–Holstein type Hamiltonian [14]

$$H^{(\mathrm{epc})} = \sum_{i=1}^{N} \sigma_i b_i^\dagger b_i \otimes \left[R_{i+1} - R_{i-1} \right] = \sum_{i=1}^{N} b_i^\dagger b_i \otimes \left[\bar{\sigma}_i \left(c_{i+1}^\dagger + c_{i+1} \right) - \bar{\bar{\sigma}}_i \left(c_{i-1}^\dagger + c_{i-1} \right) \right] \tag{7}$$

where the coupling constants $\sigma_i = \mathrm{d}\alpha_i/\mathrm{d}(R_{i+1} - R_{i-1})$ give the linearized dependence of the exciton energies α_i on the sum of the NN distances to the left and to the right of each site. The bar notation is used here to convert the EPC constants to second quantization, $\bar{\sigma}_i = \sigma_i/\sqrt{2m_{i+1}\tilde{\nu}_{i+1}}$ and $\bar{\bar{\sigma}}_i = \sigma_i/\sqrt{2m_{i-1}\tilde{\nu}_{i-1}}$. Note that in our previous work [22], the distinction between EPC constants with bars and double bars was missing, which, however, is not required for the homogeneous systems mainly investigated there.

This symmetric formulation of the EPC is suitable in case of a mirror symmetry of the individual sites frequently occurring in semiconductor materials whereas one-sided expressions are typically used for excitons in protein helices where an amide I vibration couples much more strongly to the directly adjacent H-bond [69, 70, 27]. For other model assumptions, including Peierls type models based on an R–dependence of the NN coupling parameters β_i, see our previous work [22].

3 Tensor train decompositions

3.1 Statement of the problem

Quantum dynamics of non-relativistic, closed systems (i.e., without dissipation or dephasing) is given in terms of the time-dependent Schrödinger equation (TDSE)

$$\mathrm{i}\frac{\mathrm{d}}{\mathrm{d}t}\Psi(t) = H\Psi(t), \tag{8}$$

where t is the time and where we restrict ourselves to time-independent Hamiltonians H, in our case the Hamiltonian given in Eq. (1). Note that atomic units with $\hbar = 1$ are used throughout this work. The initial quantum state is given by $\Psi(t = 0) = \Psi_0$, which in typical photophysical or photochemical simulation scenarios describes a state prepared by the interaction with light. Let us assume that a coupled excitonic-phononic state vector for each of the constituent sites will be given by a vector in the product Hilbert space

$$\psi_i \in \mathcal{H}_i := \mathcal{H}_i^{(\mathrm{ex})} \otimes \mathcal{H}_i^{(\mathrm{ph})} \cong \mathbb{C}^{d_i} \tag{9}$$

with dimension $d_i := d_i^{(\mathrm{ex})} d_i^{(\mathrm{ph})}$, where $d_i^{(\mathrm{ex})}$ and $d_i^{(\mathrm{ph})}$ are the dimensions of the Hilbert spaces of excitonic and vibrational state vectors, respectively. Then, time-dependent quantum state vectors $\Psi(t)$ of a complete chain (or ring) comprising N sites can be understood as tensors of order N,

$$\Psi \in \mathcal{H} := \mathcal{H}_1 \otimes \mathcal{H}_2 \otimes \cdots \otimes \mathcal{H}_N \cong \mathbb{C}^D \tag{10}$$

with a total dimension of $D := \prod_{i=1}^N d_i$, i.e., the numerical discretization of Ψ is a tensor in $\mathbb{C}^{d_1\times\cdots\times d_N}$. In analogy, the tensorized representation H of the (real-valued, symmetric) Hamiltonian given in Eq. (1) is a tensor in $\mathbb{R}^{(d_1\times d_1)\times\cdots\times(d_N\times d_N)}$.

Because the formal time evolution of quantum states

$$\Psi(t) = \exp(-\mathrm{i}tH)\Psi_0 \tag{11}$$

is not computationally available for large N, our aim is to numerically integrate the TDSE (8) in terms of tensor representations by employing time integrators. In general, however, the storage consumption of (non-sparse) tensors of the form (1) or (10) grows exponentially with the order N. Due to this so-called *curse of dimensionality*, storing the considered tensors in full format may be not feasible for large N. Therefore, special tensor representations are required. As in [22], we will focus on the *tensor train format* (TT format) [58, 60]. This type of tensor decomposition is not only tailor-made for chain-like topologies such as our Hamiltonians with NN interactions, but it is also a preferred choice for representing high-dimensional tensors in terms of storage consumption and computational robustness. We will also introduce properly designed numerical methods based on tensor trains which we will use to solve evolution equations such as the TDSE (8) in high-dimensional tensor spaces which otherwise would be extremely expensive or even impossible with today's computational resources.

3.2 Tensor trains and SLIM decomposition

In this work, the TT format is used to represent a quantum state Ψ. That is, we decompose a tensor in $\mathbb{C}^{d_1 \times \cdots \times d_N}$ into N component tensors which are coupled in a chain, see Fig. 1 and Def. 1.

Figure 1: *Graphical representation of tensor trains: Tensors are depicted as circles with different arms indicating the set of free indices. (a) Tensor of order 5 in TT format, the first and the last core are matrices, the other cores are tensors of order 3. (b) Linear operator in TT format, the first and the last core are tensors of order 3, the other cores are tensors of order 4. In both cases, arms corresponding to first and last TT ranks are omitted since* $r_0 = r_5 = 1$.

Definition 1 *A tensor* $\Psi \in \mathbb{C}^{d_1 \times d_2 \times \cdots \times d_N}$ *is said to be in the TT format if*

$$\Psi = \sum_{k_0=1}^{r_0} \cdots \sum_{k_N=1}^{r_N} \Psi^{(1)}_{k_0,:,k_1} \otimes \cdots \otimes \Psi^{(N)}_{k_{N-1},:,k_N}. \tag{12}$$

The tensors $\Psi^{(i)} \in \mathbb{C}^{r_{i-1} \times d_i \times r_i}$ *of order* 3 *are called TT cores and the numbers* r_i *are called TT ranks. It holds that* $r_0 = r_N = 1$ *and* $r_i \geq 1$ *for* $i = 1, \dots, N-1$.

To reduce the memory consumption as well as the computational costs, we are especially interested in low-rank TT decompositions. In Ref. [22], we used the TT format to represent stationary quantum states, i.e., solutions of the TISE. Here, we are interested in the numerical solution of Eq. (8) in form of a time series $(\Psi(t_0), \Psi(t-1), \dots, \Psi(T))$ of TT representations. That is, if the quantum states at the considered time points can be approximated accurately enough by tensor trains with ranks of manageable size, we are able to mitigate the curse of dimensionality. For more details about the TT format, we refer to Refs. [58, 60, 59].

Since the efficiency of the tensor-based integrators described in the following sections also depends on the ranks of the operator $H \in \mathbb{R}^{(d_1 \times d_1) \times \cdots \times (d_N \times d_N)}$, we want to construct low-rank TT representations of the Hamiltonian tensor as well. All terms of the Hamiltonians introduced in Sec. 2 either act locally on a single site or on two neighboring sites. Thus, as we explained in Ref. [22], H can be expressed in the TT format by using a so-called SLIM decomposition [24]:

$$
\begin{aligned}
H = \llbracket S_1 \quad L_1 \quad I_1 \quad M_1 \rrbracket \otimes \left\llbracket \begin{matrix} I_2 & 0 & 0 & 0 \\ M_2 & 0 & 0 & 0 \\ S_2 & L_2 & I_2 & 0 \\ 0 & 0 & 0 & J_2 \end{matrix} \right\rrbracket \otimes \dots \\
\dots \otimes \left\llbracket \begin{matrix} I_{N-1} & 0 & 0 & 0 \\ M_{N-1} & 0 & 0 & 0 \\ S_{N-1} & L_{N-1} & I_{N-1} & 0 \\ 0 & 0 & 0 & J_{N-1} \end{matrix} \right\rrbracket \otimes \left\llbracket \begin{matrix} I_N \\ M_N \\ S_N \\ L_N \end{matrix} \right\rrbracket .
\end{aligned}
\tag{13}
$$

Above, we use the core notation of the TT format, cf. Refs. [40, 24, 22]. The single-site components S_i for $i = 1, \dots, N$, see Eqs. (2,4), are given by

$$
S_i = \alpha_i b_i^\dagger b_i + \tilde{\nu}_i \left(c_i^\dagger c_i + \frac{1}{2} \right) \tag{14}
$$

The NN interactions are represented by the components L_i and M_{i+1} defined as

$$
\begin{aligned}
\llbracket L_i \rrbracket &= \llbracket L_{i,1} \quad \dots \quad L_{i,\xi_i} \rrbracket & \in \mathbb{R}^{1 \times d_i \times d_i \times \xi_i}, \\
\llbracket M_{i+1} \rrbracket &= \llbracket M_{i+1,1} \quad \dots \quad M_{i+1,\xi_i} \rrbracket^{\mathbb{T}} & \in \mathbb{R}^{\xi_i \times d_{i+1} \times d_{i+1} \times 1},
\end{aligned}
$$

for $i = 1, \dots, N-1$, and

$$
\begin{aligned}
\llbracket L_N \rrbracket &= \llbracket L_{N,1} \quad \dots \quad L_{N,\xi_N} \rrbracket^{\mathbb{T}} & \in \mathbb{R}^{\xi_N \times d_N \times d_N \times 1}, \\
\llbracket M_1 \rrbracket &= \llbracket M_{1,1} \quad \dots \quad M_{1,\xi_d} \rrbracket & \in \mathbb{R}^{1 \times d_1 \times d_1 \times \xi_N},
\end{aligned}
\tag{15}
$$

for the case of cyclic systems only.

The two-site contributions to the total Hamiltonian, see Eqs. (2,4,7), are expressible in terms of five operators $L_{i,\lambda}$ acting on site i and five corresponding operators $M_{i+1,\lambda}$ acting on the neighboring site $i+1$:

$$
\begin{aligned}
L_{i,1} &= \beta_i b_i^\dagger, & M_{i+1,1} &= b_{i+1}, \\
L_{i,2} &= \beta_i b_i, & M_{i+1,2} &= b_{i+1}^\dagger, \\
L_{i,3} &= -\tilde{\omega}_i \left(c_i^\dagger + c_i \right), & M_{i+1,3} &= c_{i+1}^\dagger + c_{i+1}, \\
L_{i,4} &= \bar{\sigma}_i b_i^\dagger b_i, & M_{i+1,4} &= c_{i+1}^\dagger + c_{i+1}, \\
L_{i,5} &= -\left(c_i^\dagger + c_i \right), & M_{i+1,5} &= \bar{\bar{\sigma}}_{i+1} b_{i+1}^\dagger b_{i+1}.
\end{aligned}
\tag{16}
$$

If certain coefficients vanish, e.g., if we consider purely excitonic or phononic Hamiltonians, the numbers ξ_i of two-site interactions may even be smaller, leading to reduced TT ranks of the Hamiltonian. A detailed derivation of the above components was given in Ref. [22]. Besides the fact that the storage consumption scales only linearly with the number of sites if we consider systems with a fixed/bounded number of NN contributions, the repeating pattern of the SLIM decomposition allows us to easily increase or decrease the number of sites. We only have to insert or remove certain TT cores, respectively.

3.3 Higher-order differencing schemes

The simplest way to integrate the TDSE (8) forward by one time step Δt is to employ an explicit Euler method

$$
\Psi(t + \Delta t) = \Psi(t) - \mathrm{i} \Delta t \mathbf{H} \Psi(t) + \mathcal{O}(\Delta t^2) \tag{17}
$$

which is known to be unstable because neither the time reversal symmetry nor the symplecticity of the TDSE is conserved. However, when combining Euler steps forward and backward in time, one arrives at the second order *symmetric Euler* (S2) method

$$\Psi(t+\Delta t) = \Psi(t-\Delta t) - 2\mathrm{i}\Delta t\mathbf{H}\Psi(t) + \mathcal{O}(\Delta t^3) \tag{18}$$

which has been in use for more than 40 years in numerical quantum dynamics where it is known as *second order differencing* scheme [1, 47]. Not requiring a special structure of the Hamiltonian (such as the separability, see Sec. 3.4), the S2 scheme is universal and very simple to implement. In passing, we note the analogy with the Verlet integrator often used for numerical integration of Newton's classical equation of motion [77]. Even though this explicit propagation scheme has the advantages of being time-reversible and conditionally stable, it is neither symplectic nor strictly unitary nor energy conserving [10]. However, in practice norm and energy conservation are approximately realized for small enough time steps Δt. Since the above method is a two step method, it requires two initial conditions: (i) $\Psi(t)$, which is given, and (ii) $\Psi(t-\Delta t)$, which we obtain by propagating backwards in time. A common way to achieve this is to start by a first-order scheme (17) for half a time step, and then use the S2 scheme (18) to propagate backward another half step [47].

Higher order schemes are based on Euler methods of order $\ell_{\max}$ forward $(t+\Delta t)$ and backward $(t-\Delta t)$ in time

$$\Psi(t\pm\Delta t) = \sum_{\ell=0}^{\ell_{\max}} \frac{1}{\ell!} \left(\mp\mathrm{i}\Delta t\mathbf{H}\right)^{\ell} \Psi(t) + \mathcal{O}(\Delta t)^{\ell_{\max}+1} \tag{19}$$

Combining the forward and backward equation then yields time reversible schemes

$$\Psi(t+\Delta t) = \Psi(t-\Delta t) + \underbrace{\sum_{k=1}^{k_{\max}} \frac{2}{(2k-1)!} \left(-\mathrm{i}\Delta t\mathbf{H}\right)^{2k-1}}_{=:\mathbf{A}} \Psi(t) + \mathcal{O}(\Delta t)^{2k_{\max}+1} \tag{20}$$

which offer the advantage of eliminating all even powers of Δt, in particular the term with $\mathcal{O}(\Delta t)^{2k_{\max}}$. Hence, the resulting schemes are of order $2k_{\max}$, and they will be referred to as S2, S4, S6 for $k_{\max}=1,2,3$ throughout Sec. 4.

In our practical work using TT representations of state vectors and (Hamiltonian) operators, solving Eq. (18) or Eq. (20) is straightforward: given $\Psi(t)$, $\Psi(t-\Delta t)$ and $\mathbf{H}$ in the TT format, we can obtain $\Psi(t+\Delta t)$ by simple tensor additions and multiplications. However, since TT ranks add under addition and multiply under multiplication, we have

$$\text{rank}(\Psi(t+\Delta t)) = \text{rank}(\Psi(t-\Delta t)) + \text{rank}(\mathbf{H}) \cdot \text{rank}(\Psi(t)) \tag{21}$$

already for the second order scheme of Eq. (18). For the higher-order schemes of (20), the rank of $\mathbf{H}$ in Eq. (21) has to be replaced by rank$(\mathbf{A}) \leq \sum_{k=1}^{k_{\max}}$ rank$(\mathbf{H})^{2k-1}$ where $\mathbf{A}$ is defined in the underbrace of Eq. (20). Hence, the rank of our approximate $\Psi(t)$ would grow exponentially with the number of time steps and would become exceedingly large already after very few time steps. Therefore, one needs to perform a rank reduction after every time step, i.e., we approximate the high-rank $\Psi(t+\Delta t)$ resulting from the propagation step with a low-rank TT. That is, given a core of $\Psi(t+\Delta t)$, we reshape it into a matrix and then apply a truncated singular value decomposition (SVD). Depending on the direction of the orthonormalization, the left- or right-singular vectors then define the updated cores and the non-orthonormal part is contracted with the next core, see [59, 22] for details. Applying this procedure successively to each core from one end to the other, we obtain a low-rank approximation which is then used for the next time step. The rank reduction requires $N-1$ singular value decompositions on matrices of size $s \times d \cdot s'$ where d is local Hilbert space dimension and s and $s' \leq s$ are the maximum TT ranks of $\Psi(t+\Delta t)$ before and after the orthonormalization. The total cost in each time step can be estimated by $\mathcal{O}(NR^2r^2d^2 + NR^3r^3d)$, where R and r are the maximum TT ranks of $\mathbf{A}$ and $\Psi(t)$, respectively. The first term results from estimating the contraction of $\mathbf{A}$, see Eq. (20), with $\Psi(t)$, whereas the second term corresponds to the truncation/orthonormalization of the tensor cores of $\Psi(t-\Delta t) + \mathbf{A}\Psi(t)$.

3.4 Higher order splitting schemes

Since the early days of numerical quantum dynamics, splitting approaches have been widely used for the matrix exponential (11) governing the formal solution of the TDSE [20, 19]. These methods are suitable wherever the quantum-mechanical Hamiltonian can be decomposed into (two or more) exactly (or, at least, easily) solvable parts, e.g., the kinetic and potential energy operator. Because these parts of the Hamiltonian typically don't commute, deriving approximations to the Baker–Campbell–Hausdorff formula has lead to a hierarchy of exponential splitting methods for use as integrators in solving the time discretized TDSE which are explicit and easy to implement. Based on the classical first order Lie–Trotter (LT) and second order Strang–Marchuk (SM) schemes, higher-order methods can be obtained as compositions of the basic methods [80, 73, 2, 5]. For a systematic overview of such composition methods, the reader is referred to section V.3 of Ref. [30]. Common advantages of the exponential splitting methods are that they typically are unitary, symplectic and time-reversible [49, 63].

In what follows, we construct various splitting schemes for Hamiltonians restricted to NN interactions in quasi one-dimensional chains. Moreover, we assume that all state vectors and Hamiltonian operators are given in TT format as SLIM decompositions. Splitting methods have been considered for operators in TT format, see, e.g., [57], where the case of Lie–Trotter splitting is explained in detail. In the closely related context of *density matrix renormalization group* (DMRG), TT/MPS decompositions are used to construct *time-evolving block decimation* (TEBD) schemes for propagations of quantum state vectors [78, 61], which resemble the techniques described below. For other closely related splitting methods on TTs, we refer to [50, 51].

The key to splitting the exponential in the evolution (11) is to separate the operators constituting the Hamiltonian (1) into groups as large as possible. At the same time, all the operators belonging to one group should commute with each other such that corresponding computations can be carried out in parallel [78]. Thus, for an implementation of splitting methods for TTs using SLIM decomposition (13), all single site operators S commute by construction, and operators L and M acting on odd/even NN pairs commute within their oddity groups. More specificially, we can split our Hamiltonian tensor operator $H \in \mathbb{R}^{(d_1 \times d_1) \times \cdots \times (d_N \times d_N)}$ into two parts H_{odd} and H_{even} which are defined by

$$
\begin{aligned}
H_{\text{odd}} &= \sum_{\substack{i=1,\\ i \text{ odd}}}^{N} I^{1:i-1} \otimes S^{(i)} \otimes I^{i+1:N} + \sum_{\substack{i=1,\\ i \text{ odd}}}^{N-1} I^{1:i-1} \otimes \llbracket L^{(i)} \rrbracket \otimes \llbracket M^{(i+1)} \rrbracket \otimes I^{i+2:N} \\
&= \sum_{i=1}^{\lceil \frac{N}{2} \rceil} I^{1:2i-2} \otimes S^{(2i-1)} \otimes I^{2i:N} + \sum_{i=1}^{\lceil \frac{N-1}{2} \rceil} I^{1:2i-2} \otimes \llbracket L^{(2i-1)} \rrbracket \otimes \llbracket M^{(2i)} \rrbracket \otimes I^{2i+1:N}
\end{aligned}
$$

and

$$\begin{aligned}H_{\text{even}} &= \sum_{\substack{i=1,\\ i \text{ even}}}^{N} I^{1:i-1} \otimes S^{(i)} \otimes I^{i+1:N} + \sum_{\substack{i=1,\\ i \text{ even}}}^{N-1} I^{1:i-1} \otimes [\![L^{(i)}]\!] \otimes [\![M^{(i+1)}]\!] \otimes I^{i+2:N} \\ &= \sum_{i=1}^{\lfloor \frac{N}{2} \rfloor} I^{1:2i-1} \otimes S^{(2i)} \otimes I^{2i+1:N} + \sum_{i=1}^{\lfloor \frac{N-1}{2} \rfloor} I^{1:2i-1} \otimes [\![L^{(2i)}]\!] \otimes [\![M^{(2i+1)}]\!] \otimes I^{2i+2:N},\end{aligned}$$

respectively. Next, we define H_i, $i = 1, \dots, N-1$, to denote the components

$$\begin{aligned}H_i &= I^{1:i-1} \otimes S^{(i)} \otimes I^{i+1:N} + I^{1:i-1} \otimes L^{(i)} \otimes M^{(i+1)} \otimes I^{i+2:N} \\ &= I^{1:i-1} \otimes \left(S^{(i)} \otimes I^{(i+1)} + L^{(i)} \otimes M^{(i+1)} \right) \otimes I^{i+2:N},\end{aligned}$$

whereas the last component with $i = N$ is simply given by

$$H_N = I^{1:N-1} \otimes S^{(N)}.$$

Note that we here only consider non-cyclic systems because defining $H_N = I^{1:N-1} \otimes S^{(N)} + M_1 \otimes J^{2:N_1} \otimes L_N$, cf. (13), would either lead to a significant increase of the computational complexity of the following schemes or would involve cyclic TT representations [28] of quantum states, both of which are beyond the scope of the present work. For the use of SLIM decompositions of cyclic systems, we refer to [24, 22]. With this definition of the H_i, the tensors H_{odd} and H_{even} can then be written as

$$H_{\text{odd}} = \sum_{i \in \mathcal{I}_{\text{odd}}} H_i, \quad \mathcal{I}_{\text{odd}} = \{1, 3, \dots, 2\lceil N/2 \rceil - 1\} \tag{22}$$

and

$$H_{\text{even}} = \sum_{i \in \mathcal{I}_{\text{even}}} H_i, \quad \mathcal{I}_{\text{even}} = \{2, 4, \dots, 2\lfloor N/2 \rfloor\}. \tag{23}$$

The components of H_{odd} as given in (22) commute pairwise. The same holds for the components of H_{even} as given in (23). This implies that the components of the propagator in Eq. (11) can be expressed as

$$\begin{aligned}\exp(-\mathrm{i}tH_{\text{odd}}) &= \prod_{i \in \mathcal{I}_{\text{odd}}} \exp(-\mathrm{i}tH_i) \\ &= \prod_{i \in \mathcal{I}_{\text{odd}}} I^{1:i-1} \otimes \exp\left(-\mathrm{i}t \left(S^{(i)} \otimes I^{(i+1)} + L^{(i)} \otimes M^{(i+1)} \right)\right) \otimes I^{i+2:N}\end{aligned}$$

with $I_{N+1} = 1$ and $M_{N+1} = 0$, see above. An analogous statement holds for $\exp(-\mathrm{i}tH_{\text{even}})$. That is, the tensor exponentials of $-\mathrm{i}tH_{\text{odd}}$ and $-\mathrm{i}tH_{\text{even}}$ can be written as the product of $\lceil N/2 \rceil$ and $\lfloor N/2 \rfloor$, respectively, commuting tensor operators acting only on two sites at most. Thus, we can directly implement splitting schemes such as first-order Lie–Trotter (LT) or second-order Strang–Marchuk (SM), see Fig. 2, given by

$$\exp(-\mathrm{i}tH) \overset{\text{LT}}{\approx} \exp(-\mathrm{i}tH_{\text{odd}}) \exp(-\mathrm{i}tH_{\text{even}})$$

and

$$\exp(-\mathrm{i}tH) \overset{\text{SM}}{\approx} \exp\left(-\mathrm{i}\frac{t}{2}H_{\text{odd}}\right) \exp(-\mathrm{i}tH_{\text{even}}) \exp\left(-\mathrm{i}\frac{t}{2}H_{\text{odd}}\right),$$

respectively.

The SM split-operator approach offers the advantage of being unitary, symplectic, stable, symmetric, and time-reversible [19], However, to obtain highly accurate results, this algorithm requires using small time steps because it has only second-order accuracy. Hence, we consider TT-based splitting schemes with higher order by using the fact that these methods can be obtained as suitable compositions of SM steps [63], i.e.,

$$\exp(-\mathrm{i}tH) = \mathsf{SM}(-\mathrm{i}\gamma_s tH)\cdots\mathsf{SM}(-\mathrm{i}\gamma_1 tH)$$

with

$$\mathsf{SM}(-\mathrm{i}\gamma tH) := \exp\left(-\mathrm{i}\frac{\gamma t}{2}H_{\mathsf{odd}}\right)\exp(-\mathrm{i}\gamma tH_{\mathsf{even}})\exp\left(-\mathrm{i}\frac{\gamma t}{2}H_{\mathsf{odd}}\right),$$

where s is the number of stages and where consistency implies that $\sum_{j=1}^{s}\gamma_j = 1$. For more information see Ref. [49], where an overview of splitting methods with different order is given. In the present work, we consider the palindromic Yoshida–Neri (YN, order 4 with 3 stages) [80] and Kahan–Li (KL, order 8 with 17 stages) [36] compositions with coefficients

$$\gamma_1 = \gamma_3 = 1.3512, \quad \gamma_2 = -1.7024,$$

and

$$\begin{aligned}
\gamma_1 = \gamma_{17} = \quad 0.1302, \quad \gamma_2 = \gamma_{16} = 0.5612, \quad \gamma_3 = \gamma_{15} = -0.3895, \quad \gamma_4 = \gamma_{14} = 0.1588,\\
\gamma_5 = \gamma_{13} = -0.3959, \quad \gamma_6 = \gamma_{12} = 0.1845, \quad \gamma_7 = \gamma_{11} = \quad 0.2584, \quad \gamma_8 = \gamma_{10} = 0.2950,\\
\gamma_9 = -0.6055,
\end{aligned}$$

respectively. Because some of the coefficients are negative, both the YN and the KL scheme can be considered as combinations of backward and forward propagations in time.

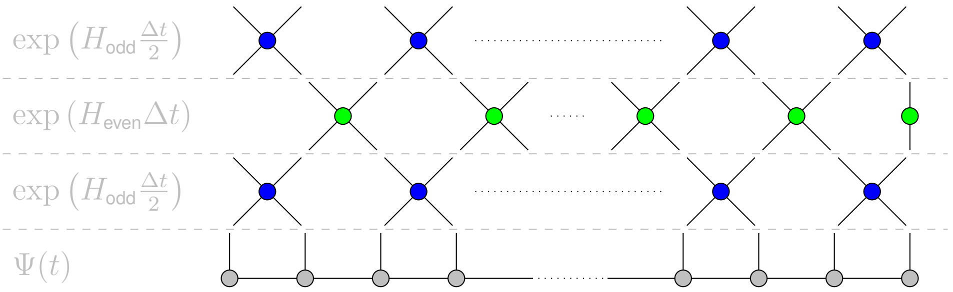

Figure 2: *Strang splitting for SLIM operators for even number N of sites: In each stage of the splitting scheme, only pairs of cores or single cores are altered. If no rank reduction is performed between these stages, the ranks of the resulting TT representation of $\Psi(t+\Delta t)$ are bounded by rd^3, where r is the maximum TT rank of $\Psi(t)$.*

Note that the composition schemes described above are time-reversible, symplectic and unitary, i.e., norm-preserving. In analogy to the higher-order differencing schemes, see Sec. 3.3, the advantages of TT-based splitting methods are that, in contrast to implicit time-integration methods, we do not have to rely on iterative solvers for linear systems like the *alternating linear scheme* (ALS) [33] and we can, in principle, parallelize the tensor contractions and rank reductions in each stage. In particular, homogeneous systems can be efficiently simulated by splitting methods since the two-site tensor exponentials of H_{odd} and H_{even} are identical for all sites. In general, each two-site operator $\exp(\mathrm{i}tH_i)$ has a TT representation with rank bounded by d^2. Thus, by orthonormalizing (without truncation, see Sec. 3.3) between the stages, the ranks of the resulting tensor after one SM step are alternately bounded by rd^2 and rd^3. In this case, the computational complexity for sufficiently large N can be estimated by $\mathcal{O}(Nr^3d^8)$, where we assume that in each stage the matricizations of the two-site operators are multiplied by the contractions of the corresponding cores and the resulting matrix is reshaped and decomposed by using an SVD. Note that a subsequent truncation for reducing the ranks of $\Psi(t+\Delta t)$ to r would take $O(Nr^3d^5)$ floating-point operations. However, if we only allow TT ranks bounded by some number $s < rd$ between the SM stages, we can reduce the computational costs to $O(Ns^3d^4)$. Truncating the ranks of the resulting tensor train to r then only takes $O(Nrs^2d)$ operations. In this way, we can significantly reduce the computational complexity but we have to accept losses in accuracy since our experiments showed that higher TT ranks are needed particularly in between the SM stages. Choosing $s = 2r$, however, turned out to yield nearly the same numerical results in our test cases as when allowing arbitrarily large TT ranks in between the SM stages.

3.5 Software

All simulations presented in this work are carried out using our recently developed Python package WAVETRAIN which is publicly available via the GitHub platform [62]. It encompasses various numerical solvers for TISE and TDSE for Hamiltonians in TT form using a SLIM representation, among them all the integrators mentioned in the present work. WAVETRAIN builds on SCIKIT-TT [25], an open-source tensor train toolbox for Python based on NumPy and SciPy. For short chains, $N \leq 5$, our results obtained with WAVETRAIN are in excellent agreement with values obtained from the conventional, grid-based solvers for general Hamiltonians available within the WAVEPACKET software package [67, 65, 66].

4 Results and Discussion

In this Section, we aim at assessing the performance and accuracy of the TT techniques, in particular the various propagators to numerically solve the TDSE for excitons, for phonons, as well as for the coupled systems. First of all, our comparisons are based on the conservation of norm and energy over time. Where possible, we also compare our numerical results with semi-analytical solutions which are available for short chains, see Sec. 4.3, and/or for harmonic phonons, see Sec. 4.4.

4.1 Model parameters

Unless stated otherwise, in our computer experiments we restrict ourselves to the case of non-periodic, homogeneous chains, with the model parameters $\alpha, \beta, m, \nu, \omega, \sigma$ being equal for all sites, with their numerical values adapted from our previous work [22]. For the excitonic Hamiltonian of (2), we choose a local excitation energy $\alpha = 0.1E_h$ (≈ 2.7 eV) which is of the order of typical band gaps in organic semiconductors, whereas the NN coupling energy is chosen one order of magnitude smaller, $\beta = -0.01E_h$. The phononic Hamiltonian of (3) is parametrized in terms of mass-weighted displacement coordinates, $\tilde{R} = \sqrt{m}R$, here with unit masses, $m = 1$, and harmonic frequencies $\nu = 10^{-3}E_h/\hbar$ (≈ 220 cm^{-1}) and $\omega = \sqrt{2} \times 10^{-3}E_h/\hbar$ for the restraining and for the NN oscillators, respectively. The coupling constant occurring in the (symmetric) EPC mechanism of Eq. (7) is chosen even smaller than the vibrational frequencies, $\sigma = 2 \times 10^{-4}E_h/a_0$. Note that for this value of the EPC constant, the stationary states obtained as solutions of the TISE display mutual trapping of excitons and phonons, the former ones localized with a full width at half maximum of about 7 sites, see our previous work [22]. Note that the use of mass-weighted coordinates implies a scaling of the EPC constant with $\tilde{\sigma} = \sigma/\sqrt{m}$. Thus, it is straight-forward to transfer all our results described below to arbitrary values of the particle masses involved. Except where stated otherwise, we employ a basis set consisting of $d^{(\mathrm{ex})} = 2$ (electronic two-state model) and $d^{(\mathrm{ph})} = 8$ vibrational basis functions (from the second quantization introduced in Sec. 2).

4.2 Time scales

For a homogeneous, non-periodic chain of infinite length, the TDSE for the purely excitonic two-state Hamiltonian of Eq. (2) can be solved analytically: For the case of an initial excitation localized at site i_0, the probability of finding the exciton at time t on site i is given by

$$\mathcal{P}_i(t) = J^2_{i-i_0}(2|\beta|t) \tag{24}$$

where the J_n are n-th order Bessel functions of the first kind [41, 70]. In practice, these solutions are of limited use as a benchmark for numerical quantum dynamics because typically the excitations quickly reach the end of a finite length chain. However, the above solution is instrumental in defining a time scale for the excitonic energy transport as the time between the first maximum of J_0 (at $t = 0$) and the first maximum of J_1 (at $2|\beta|t/ \approx 1.8412$). Hence, for our example we suggest a rounded value for the time scale, $\tau^{(\mathrm{ex})} \equiv 1/|\beta| = 100$ in atomic units, or approximately 2.4 fs. In the absence of analytical results for phonon dynamics given by the Hamiltonian of Eq. (4), we simply define an analogous time scale for phononic energy transport, $\tau^{(\mathrm{ph})} \equiv 1/\nu = 1000$, or approximately 24 fs. This value approximately coincides with our empirical observations of a vibrational excitation moving from one site to its nearest neighbors. Similarly, the time scale of the exciton-phonon coupling of (7) is defined as $\tau^{(\mathrm{epc})} \equiv 1/|\sigma| = 5000$, or approximately 120 fs, characterizing the redistribution of energy between excitonic and phononic subsystems.

4.3 Comparison with quantum dynamics

For short chains, it is straight-forward to obtain semi-analytical solutions to the TDSE (8) by calculating the matrix exponential in the formal solution (11) directly. Assuming a maximum matrix size of 4096×4096, the semi-analytical approach is limited to $N = 12$, $N = 4$, or $N = 3$ for excitons with $d^{(ex)} = 2$, phonons with $d^{(ph)} = 8$, or coupled systems with $d = d^{(ex)}d^{(ph)} = 16$, respectively.

First, we run semi-analytical propagations with 100 main time steps of length $\tau^{(\mathrm{ex})}/2 = 50$ for excitons with and without EPC and $\tau^{(\mathrm{ph})}/2 = 500$ for phonons only. As expected, these simulations display preservation of norm and energy to machine precision. Subsequently, we use those results as a reference in assessing the quality of TT-based propagations of the same duration where we split the main time steps into 1, 2, 5, 10, 20, 50, 100, 200, 500, or 1000 sub-steps each. Propagations are carried out using the second order symmetric Euler (S2) method, see Sec. 3.3, as well as four different splitting schemes, i.e., Lie–Trotter (LT), Strang–Marchuk (SM), Yoshida–Neri (YN), and Kahan–Li (KL), see Sec. 3.4. In all simulations of exciton dynamics with or without EPC, the initial state corresponds to a single site near the center of the chain being excited. Our simulations of phonon dynamics were initialized with the vibration of that site being in a coherent state where a mean displacement $\langle \Delta R \rangle = 1$ has been chosen [64]. Note that this value is small enough such that the truncation of the vibrational basis (here $d^{(\mathrm{ph})} = 8$) does not have a notable influence on the precision of the results. All other sites were prepared in their excitonic and/or vibrational ground states.

Our results for the three classes of systems investigated are displayed in Figs. 3, 4, and 5. The columns of these figures correspond to different values of r, the maximum ranks of the solutions, characterizing the flexibility of the solutions. Note that for given dimension d of the Hilbert spaces for each of the N sites, the maximum rank possible, $r_{\max}$, of a tensor train (after left- and right-orthonormalization) is given by $d^{\lfloor N/2 \rfloor}$ where the values of d are chosen as 2, 8, or 16 for excitons, phonons, or coupled systems, respectively. Hence, we have $r_{\max} = 64$ both for pure excitons ($N = 12$) and pure phonons ($N = 4$) whereas we have $r_{\max} = 16$ for coupled systems ($N = 3$). The CPU times for a single thread of a Xeon Skylake 6130 processor, shown in the upper rows of the figures, increase linearly with the number of time sub-steps. Owing to the simplicity of the integrator (18), the S2 is the fastest of the 5 integrators compared here. It is followed by the first order (LT) and second order (SM) splitting schemes with slightly higher computational effort. Note that results for S2, LT, SM propagations are partly not available for the larger sub-step sizes where they become unstable. The elapsed CPU times are considerable higher for the 4-th order (YN) and 8-th order (KL) schemes.

The panels in the second rows of Figs. 3–5 show the root mean squared deviation (RMSD, averaged over the 100 time steps considered) of the norm of the quantum-mechanical states from unity. The S2 method reproduces the preservation of norm moderately well with RMSD values typically between 10^{-2} and 10^{-11}, steeply descending with decreasing step size. RMSD values between 10^{-9} and 10^{-13} are often found for the splitting methods, which is expected because of the unitarity of those schemes. However, this favorable behavior is only found where the ranks of the solutions, r, are high enough. While this is already the case for $r = 2$ for the exciton results shown in Fig. 3, one has to go close to the maximum ranks for the other two systems, i.e., $r = r_{\max} = 64$ for the phonons shown in Fig. 4 or $r = r_{\max} = 16$ for the coupled systems, see Fig. 5. A few outliers are found for the YN scheme for excitons, see Fig. 3, which are apparently caused by the rank reduction in between the SM stages, see Section 3.4.

A similar behavior is found in our (relative) RMSDs of energies w.r.t. their initial values and for the (absolute) RMSDs of the TT-based solutions from the semi-analytical solutions, as can be seen in the third and fourth rows of Figs. 3–5. Once the ranks of the solutions, r, exceed the above-mentioned thresholds, these two quantities can be brought down to 10^{-11} or even lower for small enough time steps. While such a high quality of the numerical solutions requires rather small time steps for the lower order propagators, it is reached already for much larger time steps when using the higher order schemes. As expected, our data in the last rows (RMSDs of the state vectors) of the right columns of Figs. 3–5 are well approximated by power laws with exponents of approximately 1 (LT), 2 (S2, SM), 4 (YN), and 8 (KL). The deviating behavior of the RMSDs when applying YN and KL for small time steps can be explained by the high number of SVDs used for truncating/orthonormalizing the intermediate solutions, see Sec. 3.4. In this case, the (numerical) errors induced by the core decompositions appear to outweigh the time-discretization error.

To summarize, Fig. 6 shows a synopsis of our results for excitons, phonons, and coupled systems. Again, the respective chain lengths of $N = 12$, $N = 4$, and $N = 3$ are equivalent in the sense that the dimensions of the underlying Hilbert spaces, $(d^{(ex)})^{12} = (d^{(ph)})^4 = (d^{(ex)} d^{(ph)})^3 = 4096$, are equal. In this figure, the accuracy, calculated as RMSD between semi-analytical and TT-based numerical results, is shown as a function of the total CPU time. Essentially, the comparison shows the superiority of the higher-order splitting integrators when high precision is required. Only the 4-th order (YN) and 8-th order schemes (KL) are able to reach a precision of 10^{-8} and below. The most precise results are obtained for the KL integrator, with RMSDs below 10^{-11} for suitable choice of the time step size. In particular, the CPU times required to reach the maximal precision are about 10^2 s for excitons and phonons, whereas about 10^3 s are found for the coupled systems. Since we here consider rather short chains, especially for phonons and coupled systems, we observe only a weak influence of the maximum TT rank on the computational costs. But the complexity of the simulations employing the splitting schemes still depends on d^4, see Sec. 3.4, which we identify as the reason for the higher

CPU times required for computing accurate solutions for the coupled exciton-phonon systems.

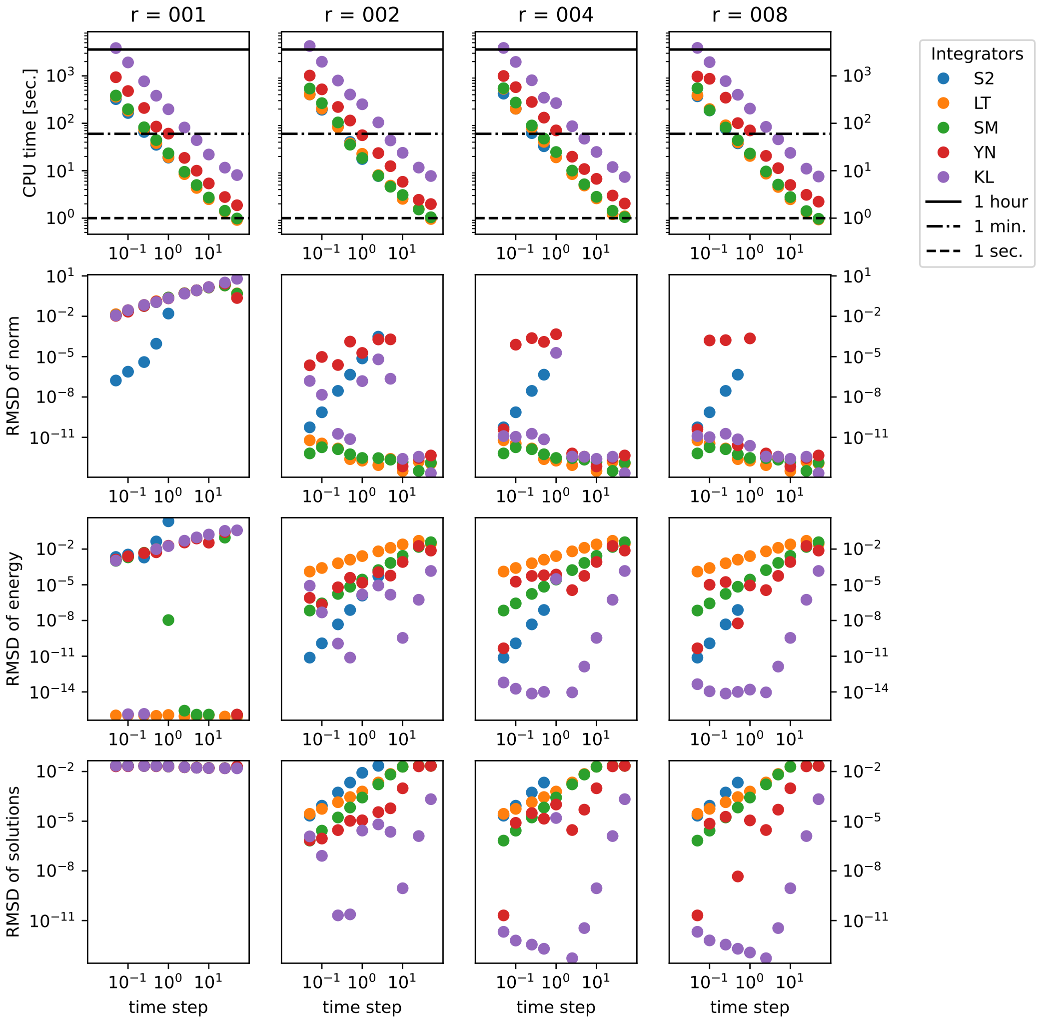

Figure 3: *Quantum dynamics of purely excitonic chains with* $d = 2$ *and* $N = 12$ *sites. From left to right: Maximum number of ranks of state vectors increasing. From top to bottom: CPU-time versus size of temporal sub-steps, deviation of norm from unity, relative deviation of energy from initial value, deviation of state vectors from semi-analytical reference data. For second order symmetric Euler (S2), Lie–Trotter (LT), Strang–Marchuk (SM), Yoshida–Neri (YN), and Kahan–Li (KL) integration methods*

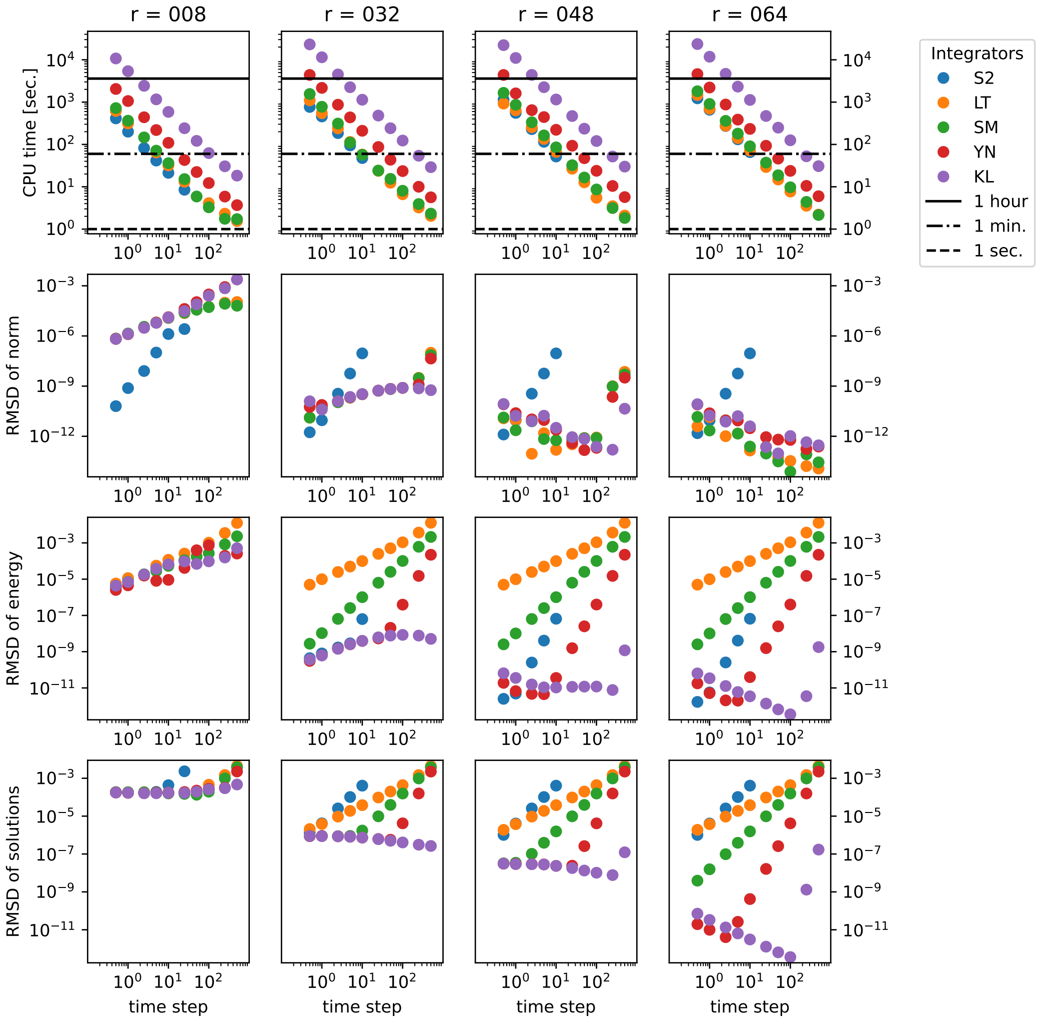

Figure 4: *Quantum dynamics of purely phononic chains with $d = 8$ and $N = 4$ sites. For details, see caption of Fig. 3*

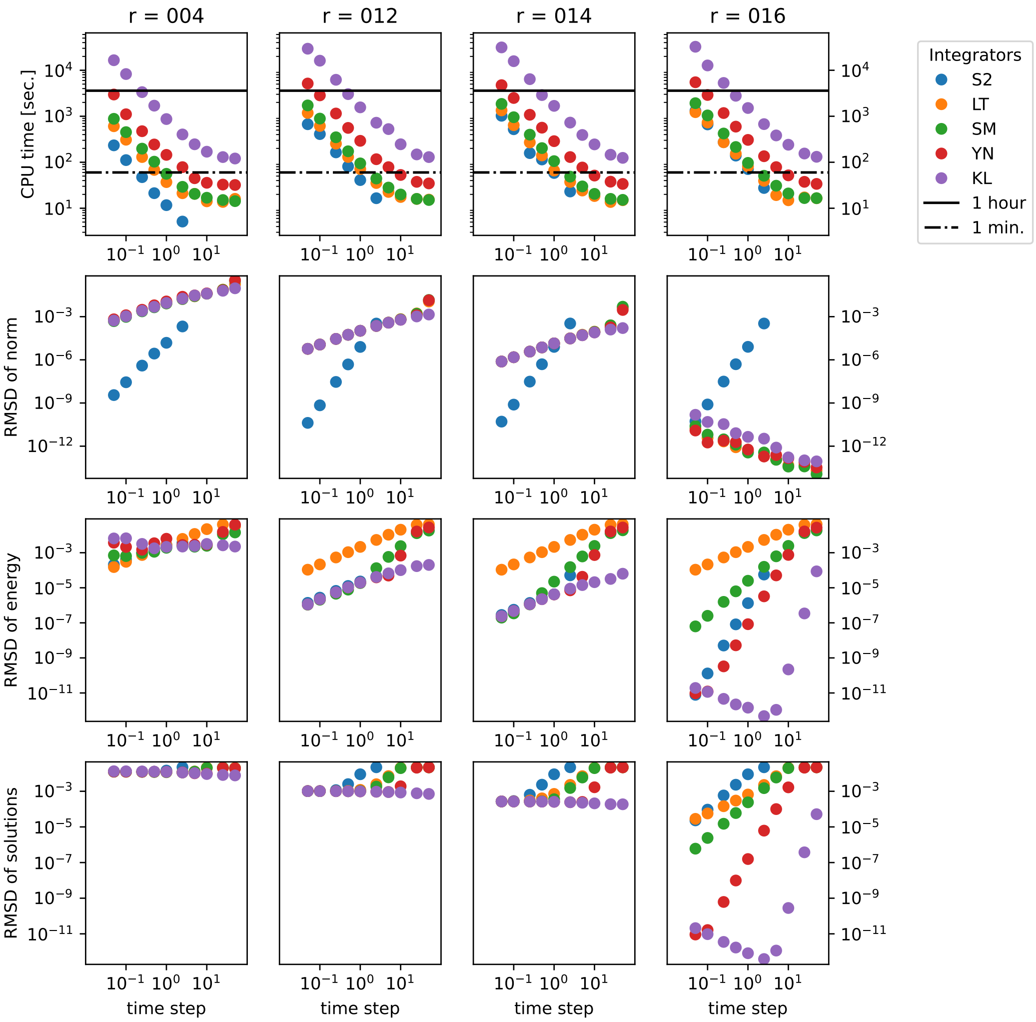

Figure 5: *Quantum dynamics of coupled excitons and phonons for $d = 16$ and $N = 3$ sites. For details, see caption of Fig. 3*

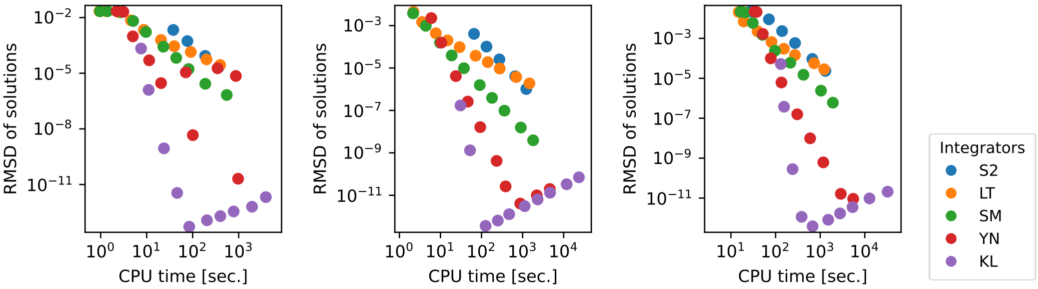

Figure 6: *Accuracy of solutions versus computational effort. From left to right: excitons ($N = 12$, $r = 8$, $d = 2$), phonons ($N = 4$, $r = 64$, $d = 8$), and coupled systems ($N = 3$, $r = 16$, $d = 16$).*

4.4 Comparison with classical dynamics

For the dynamics of phonons, reference data for assessing our TT-based results can also be generated on the basis of the quantum-classical correspondence. According to the Ehrenfest theorem, the quantum-mechanical expectation values of positions and momenta coincide with results from classical trajectories, as long as the vibrational Hamiltonian is a polynomial of order not higher than two [12]. This is indeed the case for our vibrational model Hamiltonian (3) which can be re-formulated as $H^{(\mathrm{ph})} = R^T\mathbf{F}R + P^T\mathbf{G}P$ where $\mathbf{F}$ and $\mathbf{G}$ stand for the Hessians of the Hamiltonian function with respect to positions, R, and momenta, P, respectively. Under these assumptions, Hamilton's classical equations of motion can be solved in a semi-analytical manner using a matrix exponential

$$\begin{pmatrix} R(t) \\ P(t) \end{pmatrix} = \exp\left[\begin{pmatrix} \mathbf{0} & \mathbf{G} \\ -\mathbf{F} & \mathbf{0} \end{pmatrix} t\right] \begin{pmatrix} R(0) \\ P(0) \end{pmatrix} \tag{25}$$

where a symplectic phase space formulation [30] is used and where $\mathbf{0}$ stands for a zero matrix of size $N \times N$. Our classical simulations are initialized with a single site (at the center of the chain) displaced by $\Delta R = 1$ while all other sites are at their equilibrium positions. We generate a set of classical simulations with a duration of 100 time steps of size $\tau^{(\mathrm{ph})}/2 = 500$ for $N \in \{4, 8, 16\}$. As expected for these system sizes, the semi-analytical solutions display excellent preservation of energy within machine accuracy.

Next, we conduct TT-based quantum propagations of the same duration ($50\tau^{(\mathrm{ph})} = 50000$) using both splitting (LT, SM) and differencing (S2, S4) propagators, again sub-dividing the main time steps into 1, 2, 5, 10, 20, 50, 100, 200, 500, 1000 sub-steps each. Moreover, we restrict our analysis to the results for $r = 32$. For shorter chains with $N = 4$, this value has already been shown to yield reasonable results for the RMSDs of the state vectors, see Fig. 4. Note that we here exclude the higher-order splitting schemes (YN, KL) due to the exceedingly high computational effort. Furthermore, we find that S6 as well as S8 splitting methods yield results that are almost identical to those obtained for the S4 method which is the reason why we do not show them anywhere in Fig. 7. We explain this effect as a consequence of the used orthonormalizations and rank reductions which eliminate the information stored in the terms corresponding to small singular values and expect S6 to show better results than S4 when allowing for higher TT ranks.

In analogy to our classical simulations of phonon dynamics, we initialize our quantum simulations by using a coherent state for a single site with the mean position matching the displacement given above. Our results are shown in Fig. 7 where RMSD comparisons of quantum versus classical position values of the vibrational coordinates are shown in the last row. In contrast to our simulations of phonon dynamics presented in Sec. 4.3, we use a larger basis set with $d^{(\mathrm{ph})} = 16$ here which has turned out to be mandatory when aiming at high accuracy for the comparison of vibrational coordinates.

The CPU times for the four integrators used here are shown in the top panels of Fig. 7 for chains of 4, 8, and 16 repeat units. We see an increase in the CPU times of roughly one order of magnitude upon doubling the chain length both for the differencing schemes (S2, S4) and for the splitting (LT, SM) schemes. As stated in Sec. 3.3 and Sec. 3.4, the computational complexities of the differencing and splitting schemes, respectively, scale linearly with the chain length. The reason why this behavior cannot be observed in Fig. 7 is the comparatively small number of sites and the fact that the ranks r_1 and r_{N-1} of a TT representation of a quantum state vector with dimensions d are always bounded by d. Thus, in this experiment, every tensor train with $N = 4$ has only one rank bounded by 32, whereas it has five when $N = 8$ and 13 when $N = 16$. Hence, due to the dominant computational costs of contractions and orthonormalizations of TT cores with maximum ranks, the CPU times in Fig. 7 are not expected to show a linear scaling when doubling the chain length. However, by bounding the TT ranks of the intermediate solutions in between the SM stages to $2r$, cf. Section 3.4, we are able to reduce the increase of the CPU times for splitting methods significantly while observing almost no loss in accuracy.

The behavior of the norm of the state vectors is shown in the second row of Fig. 7. The norm is preserved up to machine precision for the unitary LT and SM splitting schemes only for $N = 4$ whereas notable deviations from unity are found for $N = 8$ and $N = 16$. This behavior is attributed to the finite ranks, $r = 32$, used here, see also Fig. 4 and our discussion of rank effects in Sec. 4.3. In contrast, for the S2 and S4 differencing schemes, the norm is only approximately conserved for short time steps. For $N = 4$ and $N = 8$, the deviation from unity scales is approximately proportional to τ^{-4} for the S2 scheme as expected [1], whereas it scales as τ^{-3} for the S4 scheme. Note that the RMSDs for longer chains ($N = 16$) are much larger due to finite-rank effects.

The third row of Fig. 7 shows that the energies are not preserved exactly, as expected for our choice of integrators which are known not to conserve quadratic invariants rigorously. The comparison of our results does not show any characteristic differences between the different integrators for longer chains ($N = 8$ and $N = 16$). Only for short chains ($N = 4$), the double-logarithmic representations show an approximately linear behavior with slopes of 1.0 (LT), 2.0 (SM), 2.5 (S2) and 3.0 (S4).

Finally, we consider the deviations (RMSD) of our numerical TT quantum results for the calculated positions from our (semi-analytical) classical results described at the beginning of this section. Again, only for short chains we find straight lines in the bottom panels of Fig. 7, this time for $N = 4$ with slopes of 1.0 (LT), 2.0 (SM), 2.0 (S2) and 4.0 (S4) as expected. Also for the longer chains with $N = 8$ and $N = 16$ we find that the higher order differencing schemes are superior to the lower order ones. Except for the largest time steps, the SM scheme clearly beats the LT scheme, and the S4 scheme is often several orders of magnitude more precise than the S2 scheme which, however, is the fastest.

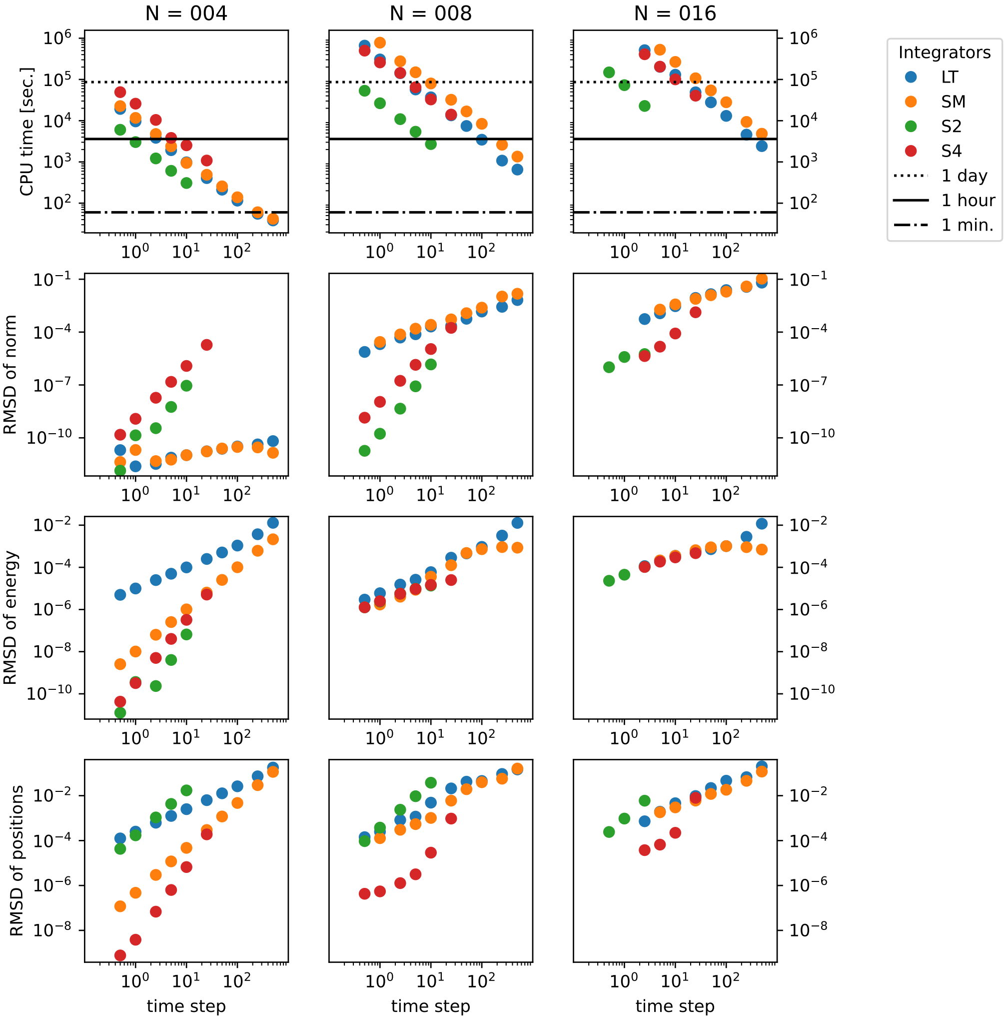

Figure 7: *Quantum dynamics of phonons for $N = 4$, $N = 8$, and $N = 16$ sites (from left to right) for $d = 16$ and $r = 32$. Note that the last row shows the RMSDs of the displacements (position coordinates) of the oscillators*

5 Conclusions and Prospects

In the present work, we have shown how to apply tensor-trains (TT) to solve the time-dependent Schrödinger equation for chain-like systems with nearest neighbor (NN) interactions only. The aim of this approach is to mitigate the curse of dimensionality, i. e., to reduce the memory consumption as well as the computational costs, as much as possible. Throughout this study, we have employed memory-efficient SLIM representations to construct TT representations of the quantum-mechanical Hamiltonians and state vectors.

Two classes of explicit integrators to solve the Schrödinger equation are investigated here. First, we consider time-symmetrized Euler integrators, see Sec. 3.3, based on the second order differencing method regularly used since the early days of numerical quantum dynamics. Second, we study splitting propagators such as the well-known first order Lie–Trotter and the second-order Strang–Marchuk schemes, see Sec. 3.4, originally based on a splitting of the Hamiltonian into kinetic and potential energy terms. However, in the present context of chain-like systems we build on a splitting of the Hamiltonian into groups of interleaved NN interactions commutating within each group. Both for the differencing and splitting methods, we have extended the traditional schemes to higher order ones.

This work presents rigorous tests of these approaches for three different classes of Hamiltonians, i.e., for two-state excitons, for harmonic acoustic phonons, and for coupled exciton-phonon systems modeled in terms of Frenkel–Fröhlich–Holstein type Hamiltonians. In particular, we have conducted extensive investigations of the influence of the TT ranks, the time step size, and the orders of the individual propagators for homogeneous and non-periodic chains of various lengths.

The focus of our studies in Sec. 4.3 is on the dependence of the conservation properties as well as the approximation quality on the maximum number of ranks, r, of the solutions. Typically we find a threshold behavior, i.e., once the number r exceeds a certain threshold, the quality of the solutions increases drastically. For the three classes of physical systems investigated here, this threshold is found at very different values of r. For example, for an excitonic chain of length $N = 12$, we find excellent agreement with semi-analytic results already for $r = 2$. This may be due to the fact that the exciton dynamics is confined to the Fock space of states with one excitation which also contains our initial state. (Note that the number of excitons is a conserved quantity because it commutes with the Hamiltonian (2)). In marked contrast, for a phononic chain of length $N = 4$, this threshold is already beyond $r = 50$. Nevertheless, we summarize that the TT-based propagators provide excellent solutions once the ranks are chosen large enough. In particular the higher order splitting methods such as the YN (4-th order) and KL (8-th order) schemes are recommended where very high precision (close to machine precision) is required.

The main objective of our studies presented in Sec. 4.4 is the dependence of the approximation quality on the number of sites, N. Here, splitting methods are not our preferred choice. Instead, differencing methods are more efficient for longer chains, i.e. the S2 scheme is the faster whereas the S4 scheme is more accurate than LT or SM splitting. However, one has to be aware that even S4 achieves only moderate precision.

As an outlook toward future work, we expect our approach to be extended to more complex scenarios than the ones investigated in the present work. For example, considering more than one vibrational degree of freedom per site into account is necessary, e.g., for realistically modeling the conformational dynamics of π-conjugated polymer chains [4, 17]. Obviously, this requires larger dimensions, d, of the local Hilbert spaces. In the practice of our approaches using TT based propagators, in that case differencing methods are expected to be superior to splitting methods because of the more favorable scaling of the computational costs with d for the former ones, see our estimates of the complexities at the end of Secs. 3.3 and 3.4.

Finally we remark that we have not discussed implicit integrators. For example, the implicit trapezoidal scheme offers the intriguing advantage of conserving quadratic invariants such as the energy associated with the Hamiltonians proposed in Sec. 2. Unfortunately, in our test calculations this integrator was found to be considerably slower than any of the explicit schemes considered. This is because it involves the solution of a large set of equations for every time step. In the context of TT techniques, this is typically done by means of the alternating linear scheme [33] which is rather time-consuming, see also our previous TISE work [22]. However, implicit schemes may become more attractive when combined with spatially and/or temporally adaptive schemes, similar to the trapezoidal rule for adaptive integration of Liouville equations (TRAIL) [34, 35].

Author declarations

Conflict of Interest

No potential conflict of interest was reported by the authors.

Data Availability

The Python and Bash scripts used to generate the simulation results shown in Figs. 3–7 are openly available in the ZENODO repository at https://doi.org/10.5281/zenodo.7351812. Moreover, we used version 1.0 of our open-source WAVETRAIN software [62], based on version 1.2 of the *scikit_tt* tensor train package, both of which are freely available from the GitHub platform at https://github.com/PGelss/.

References

[1] A. Askar and A. S. Cakmak. Explicit integration method for the time-dependent Schrödinger equation for collision problems. *The Journal of Chemical Physics*, 68(6):2794, 1978.

[2] A. D. Bandrauk and H. Shen. Higher order exponential split operator method for solving time-dependent Schrödinger equations. *Canadian Journal of Chemistry*, 70(2):555–559, 1992.

[3] M. H. Beck, A. Jäckle, G. A. Worth, and H.-D. Meyer. The multiconfiguration time-dependent Hartree (MCTDH) method: a highly efficient algorithm for propagating wavepackets. *Physics Reports*, 324(1):1–105, 2000.

[4] R. Binder, D. Lauvergnat, and I. Burghardt. Conformational Dynamics Guides Coherent Exciton Migration in Conjugated Polymer Materials: First-Principles Quantum Dynamical Study. *Physical Review Letters*, 120(22):227401, 2018.

[5] S. Blanes, F. Casas, and A. Murua. Symplectic splitting operator methods for the time-dependent Schrödinger equation. *The Journal of Chemical Physics*, 124(23):234105, 2006.

[6] F. A. Bornemann, P. Nettesheim, and C. Schütte. Quantum-classical molecular dynamics as an approximation to full quantum dynamics. *The Journal of Chemical Physics*, 105(3):1074, 1996.

[7] R. Borrelli and M. F. Gelin. Quantum electron-vibrational dynamics at finite temperature: Thermo field dynamics approach. *Journal of Chemical Physics*, 145(22), 2016.

[8] A. Bose and P. L. Walters. A Multisite Decomposition of the Tensor Network Path Integrals. *The Journal of Chemical Physics*, 156(2):024101, 2021.

[9] C. Chatzichristos, E. Kofidis, M. Morante, and S. Theodoridis. Blind fMRI source unmixing via higher-order tensor decompositions. *Journal of Neuroscience Methods*, 315:17–47, 2019.

[10] S. Choi and J. Vaníček. Efficient geometric integrators for nonadiabatic quantum dynamics. I. The adiabatic representation. *The Journal of Chemical Physics*, 150(20):204112, 2019.

[11] S. Choi and J. Vaníček. High-order geometric integrators for representation-free Ehrenfest dynamics. *The Journal of Chemical Physics*, 155(12):124104, 2021.

[12] C. Cohen-Tannoudji, B. Liu, and F. Laloe. *Quantum Mechanics*. Wiley, New York, 1977.

[13] A. S. Davydov. *Solitons in Molecular Systems*. Reidel, 1985.

[14] J. T. Devreese and A. S. Alexandrov. Fröhlich polaron and bipolaron: Recent developments. *Reports on Progress in Physics*, 72(6):066501, 2009.

[15] D. L. Dexter. A theory of sensitized luminescence in solids. *The Journal of Chemical Physics*, 21:836–850, 1953.

[16] D. L. Dexter, R. S. Knox, and T. FÃűrster. The radiationless transfer of energy of electronic excitation between impurity molecules in crystals. *physica status solidi (b)*, 34:K159–K162, 1969.

[17] F. Di Maiolo, D. Brey, R. Binder, and I. Burghardt. Quantum dynamical simulations of intra-chain exciton diffusion in an oligo (para -phenylene vinylene) chain at finite temperature. *The Journal of Chemical Physics*, 153(18):184107, 2020.

[18] A. Erol and B. Hunyadi. Chapter 12 - tensors for neuroimaging: A review on applications of tensors to unravel the mysteries of the brain. In Y. Liu, editor, *Tensors for Data Processing*, pages 427–482. Academic Press, 2022.

[19] M. D. Feit, J. A. Fleck, and A. Steiger. Solution of the Schrödinger equation by a spectral method. *Journal of Computational Physics*, 47(3):412–433, 1982.

[20] J. A. Fleck, J. R. Morris, and M. D. Feit. Time-dependent propagation of high energy laser beams through the atmosphere. *Applied Physics*, 10(2):129–160, 1976.

[21] V. M. Freixas, A. J. White, T. Nelson, H. Song, D. V. Makhov, D. Shalashilin, S. Fernandez-Alberti, and S. Tretiak. Nonadiabatic Excited-State Molecular Dynamics Methodologies: Comparison and Convergence. *Journal of Physical Chemistry Letters*, 12(11):2970–2982, 2021.

[22] P. Gelß, R. Klein, S. Matera, and B. Schmidt. Solving the time-independent Schrödinger equation for chains of coupled excitons and phonons using tensor trains. *The Journal of Chemical Physics*, 156(2):024109, 2022.

[23] P. Gelß, S. Klus, J. Eisert, and C. Schütte. Multidimensional approximation of nonlinear dynamical systems. *Journal of Computational and Nonlinear Dynamics*, 14(6):061006, 2019.

[24] P. Gelß, S. Klus, S. Matera, and C. Schütte. Nearest-neighbor interaction systems in the tensor-train format. *Journal of Computational Physics*, 341:140–162, 2017.

[25] P. Gelß, S. Klus, M. Scherer, F. Nüske, and M. Lücke. Scikit-TT. `https://github.com/PGelss/scikit_tt`, 2021.

[26] P. GelÃ§, S. Klus, Z. Shakibaei, and S. Pokutta. Low-rank tensor decompositions of quantum circuits. *arXiv:2205.09882*, 2022.

[27] D. D. Georgiev and J. F. Glazebrook. On the quantum dynamics of Davydov solitons in protein α-helices. *Physica A: Statistical Mechanics and its Applications*, 517:257–269, 2019.

[28] W. Hackbusch. *Tensor Spaces and Numerical Tensor Calculus*, volume 42. 2012.

[29] J. Haegeman, C. Lubich, I. Oseledets, B. Vandereycken, and F. Verstraete. Unifying time evolution and optimization with matrix product states. *Physical Review B*, 94(16):165116, 2016.

[30] E. Hairer, C. Lubich, and G. Wanner. *Geometric Numerical Integration*. Springer, New York, 2006.

[31] G. J. Hedley, A. Ruseckas, and I. D. W. Samuel. Light Harvesting for Organic Photovoltaics. *Chemical Reviews*, 117(2):796–837, 2017.

[32] F. L. Hitchcock. The expression of a tensor or a polyadic as a sum of products. *Journal of Mathematics and Physics*, 6:164–189, 1927.

[33] S. Holtz, T. Rohwedder, and R. Schneider. The Alternating Linear Scheme for Tensor Optimization in the Tensor Train Format. *SIAM Journal on Scientific Computing*, 34(2):A683–A713, 2012.

[34] I. Horenko and M. Weiser. Adaptive integration of molecular dynamics. *Journal of Computational Chemistry*, 24(15):1921–9, 2003.

[35] I. Horenko, M. Weiser, B. Schmidt, and C. Schütte. Fully adaptive propagation of the quantum-classical Liouville equation. *The Journal of Chemical Physics*, 120(19):8913–23, 2004.

[36] W. Kahan and R.-C. Li. Composition constants for raising the orders of unconventional schemes for ordinary differential equations. *Math. Comput.*, 66:1089–1099, 1997.

[37] E. Karahan, P. A. Rojas-LÃşpez, M. L. Bringas-Vega, P. A. ValdÃľs-HernÃąndez, and P. A. Valdes-Sosa. Tensor analysis and fusion of multimodal brain images. *Proceedings of the IEEE*, 103(9):1531–1559, 2015.

[38] N. Kargas and N. D. Sidiropoulos. Nonlinear system identification via tensor completion. In *Proceedings of the AAAI Conference on Artificial Intelligence*, volume 34, pages 4420–4427, 2020.

[39] N. Kargas and N. D. Sidiropoulos. Supervised learning via ensemble tensor completion. In *2020 54th Asilomar Conference on Signals, Systems, and Computers*, pages 196–199, 2020.

[40] V. Kazeev, O. Reichmann, and C. Schwab. Low-rank tensor structure of linear diffusion operators in the TT and QTT formats. *Linear Algebra and its Applications*, 438(11):4204–4221, 2013.

[41] V. Kenkre and S. Phatak. Exact probability propagators for motion with arbitrary degree of transport coherence. *Physics Letters A*, 100(2):101–104, 1984.

[42] S. Klus and P. Gelß. Tensor-based algorithms for image classification. *Algorithms*, 12(11):240, 2019.

[43] S. Klus, P. Gelß, S. Peitz, and C. SchÃijtte. Tensor-based dynamic mode decomposition. *Nonlinearity*, 31(7):3359–3380, 2018.

[44] R. Kosloff. Time-dependent quantum-mechanical methods for molecular dynamics. *The Journal of Physical Chemistry*, 92(8):2087–2100, 1988.

[45] J. J. Kranz and M. Elstner. Simulation of Singlet Exciton Diffusion in Bulk Organic Materials. *Journal of Chemical Theory and Computation*, 12(9):4209–4221, 2016.

[46] L.-C. Ku and S. A. Trugman. Quantum dynamics of polaron formation. *Physical Review B*, 75(1):014307, 2007.

[47] C. Leforestier, R. Bisseling, C. Cerjan, M. Feit, R. Friesner, A. Guldberg, A. Hammerich, G. Jolicard, W. Karrlein, H.-D. Meyer, N. Lipkin, O. Roncero, and R. Kosloff. A comparison of different propagation schemes for the time dependent Schrödinger equation. *Journal of Computational Physics*, 94(1):59–80, 1991.

[48] F. Lenz. The Ratio of Proton and Electron Masses. *Physical Review*, 82(4):554–554, 1951.

[49] C. Lubich. *From Quantum to Classical Molecular Dynamics: Reduced Models and Numerical Analysis.* European Mathematical Society, Zürich, 2008.

[50] C. Lubich and I. V. Oseledets. A projector-splitting integrator for dynamical low-rank approximation. *BIT Numerical Mathematics*, 54(1):171–188, 2014.

[51] C. Lubich, I. V. Oseledets, and B. Vandereycken. Time Integration of Tensor Trains. *SIAM Journal on Numerical Analysis*, 53(2):917–941, 2015.

[52] S. Mainali, F. Gatti, D. Iouchtchenko, P.-N. Roy, and H.-D. Meyer. Comparison of the multi-layer multi-configuration time-dependent Hartree (ML-MCTDH) method and the density matrix renormalization group (DMRG) for ground state properties of linear rotor chains. *The Journal of Chemical Physics*, 154(17):174106, 2021.

[53] H. D. Meyer, F. Gatti, and G. A. Worth, editors. *Multidimensional quantum dynamics: MCTDH theory and applications*. Wiley-VCH, 2009.

[54] O. V. Mikhnenko, P. W. M. Blom, and T.-Q. Nguyen. Exciton diffusion in organic semiconductors. *Energy Environ. Sci.*, 8(7):1867–1888, 2015.

[55] T. R. Nelson, A. J. White, J. A. Bjorgaard, A. E. Sifain, Y. Zhang, B. Nebgen, S. Fernandez-Alberti, D. Mozyrsky, A. E. Roitberg, and S. Tretiak. Non-adiabatic Excited-State Molecular Dynamics: Theory and Applications for Modeling Photophysics in Extended Molecular Materials. *Chemical Reviews*, 120(4):2215–2287, 2020.

[56] P. Nettesheim, F. A. Bornemann, B. Schmidt, and C. Schütte. An explicit and symplectic integrator for quantum-classical molecular dynamics. *Chemical Physics Letters*, 256(6):581–588, 1996.

[57] R. Orús. A practical introduction to tensor networks: Matrix product states and projected entangled pair states. *Annals of Physics*, 349:117–158, 2014.

[58] I. V. Oseledets. A new tensor decomposition. *Doklady Mathematics*, 80(1):495–496, 2009.

[59] I. V. Oseledets. Tensor-train decomposition. *SIAM Journal on Scientific Computing*, 33(5):2295–2317, 2011.

[60] I. V. Oseledets and E. E. Tyrtyshnikov. Breaking the curse of dimensionality, or how to use SVD in many dimensions. *SIAM Journal on Scientific Computing*, 31(5):3744–3759, 2009.

[61] S. Paeckel, T. Köhler, A. Swoboda, S. R. Manmana, U. Schollwöck, and C. Hubig. Time-evolution methods for matrix-product states. *Annals of Physics*, 411:167998, 2019.

[62] J. Riedel, P. Gelß, R. Klein, and B. Schmidt. WaveTrain: A Python package for numerical quantum mechanics of chain-like systems based on tensor trains. *arXiv:2302.03725*, 2023.

[63] J. Roulet, S. Choi, and J. Vaníček. Efficient geometric integrators for nonadiabatic quantum dynamics. II. the diabatic representation. *Journal of Chemical Physics*, 150(20):204113, 2019.

[64] W. P. Schleich. *Quantum Optics in Phase Space*. Wiley–VCH, Berlin, 2001.

[65] B. Schmidt and C. Hartmann. WavePacket: A Matlab package for numerical quantum dynamics.II: Open quantum systems, optimal control, and model reduction. *Computer Physics Communications*, 228:229–244, 2018.

[66] B. Schmidt, R. Klein, and L. Cancissu Araujo. WavePacket: A Matlab package for numerical quantum dynamics. III. QuantumâĂŘclassical simulations and surface hopping trajectories. *Journal of Computational Chemistry*, 40(30):2677–2688, 2019.

[67] B. Schmidt and U. Lorenz. WavePacket: A Matlab package for numerical quantum dynamics. I: Closed quantum systems and discrete variable representations. *Computer Physics Communications*, 213:223–234, 2017.

[68] M. Schröter, S. D. Ivanov, J. Schulze, S. P. Polyutov, Y. Yan, T. Pullerits, and O. Kühn. Exciton-vibrational coupling in the dynamics and spectroscopy of Frenkel excitons in molecular aggregates. *Physics Reports*, 567:1–78, 2015.

[69] A. C. Scott. Davydov's soliton revisited. *Physica D: Nonlinear Phenomena*, 51(1-3):333–342, 1991.

[70] A. C. Scott. Davydov's soliton. *Physics Reports*, 217(1):1–67, 1992.

[71] T. Serwatka and P.-N. Roy. Ground state of asymmetric tops with DMRG: water in one dimension. *The Journal of Chemical Physics*, 156(4):044116, 2022.

[72] E. Stoudenmire and D. J. Schwab. Supervised learning with tensor networks. In D. Lee, M. Sugiyama, U. Luxburg, I. Guyon, and R. Garnett, editors, *Advances in Neural Information Processing Systems*, volume 29. Curran Associates, Inc., 2016.

[73] M. Suzuki. Fractal decomposition of exponential operators with applications to many-body theories and Monte Carlo simulations. *Physics Letters A*, 146(6):319–323, 1990.

[74] S. A. Trugman, L.-C. Ku, and J. Bonča. JahnâĂŞTeller and the Dynamics of Polaron Formation. *Journal of Superconductivity*, 17(2):193–197, 2004.

[75] L. R. Tucker. The extension of factor analysis to three-dimensional matrices. In H. Gulliksen and N. Frederiksen, editors, *Contributions to mathematical psychology*, pages 110–127. Holt, Rinehart and Winston, 1964.

[76] J. C. Tully. Molecular dynamics with electronic transitions. *The Journal of Chemical Physics*, 93(2):1061, 1990.

[77] L. Verlet. Computer Ëxperimentsön Classical Fluids. I. Thermodynamical Properties of Lennard-Jones Molecules. *Physical Review*, 159(1):98–103, 1967.

[78] V. Volokitin, I. Vakulchyk, E. Kozinov, A. Liniov, I. Meyerov, M. Ivanchenko, T. Laptyeva, and S. Denisov. Propagating large open quantum systems towards their asymptotic states: cluster implementation of the time-evolving block decimation scheme. *Journal of Physics: Conference Series*, 1392(1):012061, 2019.

[79] W. Xie, D. Holub, T. Kubaš, and M. Elstner. Performance of Mixed Quantum-Classical Approaches on Modeling the Crossover from Hopping to Bandlike Charge Transport in Organic Semiconductors. *Journal of Chemical Theory and Computation*, 16(4):2071–2084, 2020.

[80] H. Yoshida. Construction of higher order symplectic integrators. *Physics Letters A*, 150(5–7):262–268, 1990.

[81] A. Zhugayevych and S. Tretiak. Theoretical Description of Structural and Electronic Properties of Organic Photovoltaic Materials. *Annual Review of Physical Chemistry*, 66(1):305–330, 2015.